Sains Malaysiana 55(10)(2026): 1760-1773
http://doi.org/10.17576/jsm-2026-5510-14

Synthesis, Spectral Characterization, DFT Studies, Molecular Docking, and Antibacterial Evaluation of Oxazolidinone Derivatives

(Sintesis, Pencirian Spektra, Kajian DFT, Pendokan Molekul dan Penilaian Antibakteria Terbitan Oksazolidinon)

ALI K. ALYWEE[1], HUSHAM ADIL[2], BILAL MAJID RUDAINI[3], TAMMAR HUSSEIN ALI[4] & SITI AISHAH HASBULLAH[5,*]

[1]*Nanomaterial Research Centre, University of Anbar, Al-Ramadi, 31001, Iraq*
[2]*University Headquarter, University of Anbar, Anbar, Iraq*
[3]*Department of Pharmaceutical Chemistry, College of Pharmacy, University of Anbar, Ramadi, Iraq*
[4]*Faculty of Pharmacy, University of Al Muthanna, Samawah 66001, Iraq*
[5]*Department of Chemical Sciences, Faculty of Science and Technology, Universiti Kebangsaan Malaysia, 43600 UKM Bangi, Selangor, Malaysia*

Received: 17 January 2026/Accepted: 5 October 2026

*Corresponding author; email: aishah80@ukm.edu.my

ABSTRACT

New oxazolidinone derivatives (**F1** - **F4**) were synthesized in good yield (60% - 78%) by the reaction of imines with monochloroacetic acid in tetrahydrofuran, using triethylamine as a catalyst. The synthesized compounds were characterized using spectroscopic techniques such as Fourier-transform infrared spectroscopy (FTIR) and ^{1}H, ^{13}C Nuclear Magnetic Resonance (NMR) spectroscopy. Density Functional Theory (DFT) calculations using Gaussian at B3LYP/6-311G basis set were used to determine the optimized structure and quantitative properties such as HOMO (Highest Occupied Molecular Orbital), LUMO (Lowest Unoccupied Molecular Orbital) and Energy Gap (ΔE) of the synthesized oxazolidinone derivatives. The molecular docking of the synthesized derivatives with the bacterial DNA gyrase protein (PDB: 6f86) was also studied. The antibacterial evaluation showed inhibition zones ranging from 8 to 35 mm among the active compound–bacteria combinations, with **F3** showing the highest activity against *Escherichia coli*, producing inhibition zones of 31 and 35 mm at 1.25 and 2.5 mg/mL, respectively.

Keywords: Antibacterial activities; DFT calculations; molecular docking; oxazolidinone derivative

ABSTRAK

Terbitan baharu oksazolidinon (**F1** - **F4**) telah disintesis dengan peratusan hasil yang baik (60% - 78%) melalui tindak balas antara imina dan asid monokloroasetik dalam tetrahidrofuran menggunakan mangkin trietilamina. Sebatian yang disintesis telah dicirikan menggunakan analisis spektroskopi seperti spektroskopi Fourier-transformasi inframerah (FT-IR) dan ^{1}H, ^{13}C NMR Spektroskopi Resonans Magnetik Nuklear (NMR). Pengiraan Kaedah Teori Fungsian Ketumpatan (DFT) menggunakan Gaussian pada set asas B3LYP/6-311G telah digunakan untuk menentukan struktur optimum dan ciri kuantitatif seperti HOMO (Orbital Molekul Terisi Tertinggi), LUMO (Orbital Molekul Terisi Terendah) dan Jurang Tenaga (ΔE) bagi terbitan oksazolidinon yang disintesis. Pendokan molekul dengan protein DNA girase bakteria (PDB: 6f86) turut dikaji. Penilaian antibakteria menunjukkan zon perencatan antara 8 hingga 35 mm antara gabungan kompaun-bakteria aktif dengan **F3** menunjukkan aktiviti tertinggi terhadap *Escherichia coli,* menghasilkan zon perencatan 31 dan 35 mm masing-masing pada pada 1.25 dan 2.5 mg/mL.

Kata kunci: Aktiviti antibakteria; pendokan molekul; pengiraan DFT; terbitan oksazolidinon

INTRODUCTION

Oxazolidinones are a fundamental class of five-membered heterocyclic compounds having both a nitrogen and an oxygen atom in their ring structure. These compounds have a significant application in organic and medicinal chemistry due to their unique structure and chemical reactions (Fernandes et al. 2023). Several productive synthesis methods have been discovered for their preparation from widely available starting materials, such as β-amino alcohols, amino acids, tri phosgene, urea, and chiral aziridines (Ganiu et al. 2020). A common approach includes the cyclization of β-amino alcohols with carbonyl containing materials such as triphosgene, whereas other approaches include the reaction

of epoxides with isocyanates or the cycloaddition of CO_2 with aziridines according to catalytic conditions (Rani, Das & Nagaraja 2025).

According to the biological perspective, oxazolidinones are widely recognized due to their wide antibacterial properties. These compounds act by binding to the 50S unit of the bacterial ribosome, which inhibits protein synthesis through disruption of the transferase activity (Malik et al. 2023). The first oxazolidinone antibiotic to receive Food and Drug Administration approval in the early 2000s, linezolid, showed promise in treating positive gram bacterial infections, especially those caused by strains of bacteria that were resistant to multiple drugs (Leach et al. 2011). Another approved drug derivative of oxazolidinone, which is tedizolid, has also been used to treat skin infections caused by bacteria that are resistant to treatment (Carena & Stryjewski 2020). In addition, previous structural studies have indicated that oxazolidinones can act as bio isosteres of amides, thiocarbamates, and carbamates. This increases their chemical and metabolic stability and allows them to form a hydrogen bond with biological targets (Zhao et al. 2021).

Oxazolidinone compounds are still interesting to medicinal chemists because they have lots of potential as medicines. In addition to their known antibacterial properties (Foti et al. 2021), different oxazolidinone derivatives have shown promise in several pharmacological areas, such as anticancer (Fernandes et al. 2023), antiviral (Ghosh et al. 2018), antitubercular (Zhao et al. 2020), anti-inflammatory (Fujimoto et al. 2017), and neurological conditions (Huang et al. 2016).

Recent studies have demonstrated the value of integrating experimental and computational approaches in the investigation of oxazolidinone derivatives. The synthesis and *in vitro* antimicrobial screening of oxazolidinone derivatives was performed along with DFT computations and molecular docking to obtain insights into the mechanism of their antimicrobial activity (Soni et al. 2025). Likewise, Bouzina et al. (2022) combined the synthesis and structural characterization of sulfamoyloxy-oxazolidinones with DFT, molecular docking and ADMET analyses to study the molecular and biological properties. The studies demonstrate the potential for computational tools to complement and aid in the interpretation of experimental results in oxazolidinone research.

In this study, a new oxazolidinone derivatives (**F1**-**F4**) were synthesized. The synthesised compounds were characterized using FT-IR and ^{1}H-NMR, and ^{13}C-NMR analyses. Density functional theory (DFT) calculations and molecular docking studies were performed. The antibacterial activity of the synthesized compounds was evaluated against selected Gram-positive and Gram-negative bacterial strains, targeting DNA gyrase.

EXPERIMENTAL DETAILS

MATERIAL AND PHYSICAL MEASUREMENTS

The Sigma-Aldrich company provided all the chemicals and reagents, which were of the highest quality. A digital melting point apparatus (Cole-Parmer Stuart MP-200D-HR) was used to find the melting points. All reactions were monitored with thin-layer chromatography (TLC) on Merck silica gel (60F254) plates (0.25 mm) and visualized under ultraviolet light (UV). Furthermore, structural characterization of the synthesized compounds was carried out using Fourier-transform infrared spectroscopy (FT-IR) and nuclear magnetic resonance spectroscopy (^{1}H and ^{13}C NMR) recorded on a Bruker Avance III HD 400 MHz spectrometer.

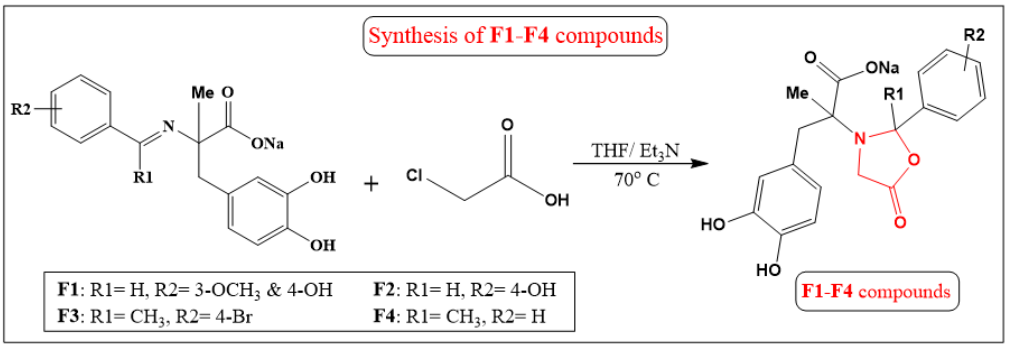
GENERAL SYNTHESIS

In a 100 mL round flask equipped with a reflux condenser, a solution of the imine derivative (0.01 mol) in 25 mL of tetrahydrofuran (THF) was added to a stirred solution of monochloroacetic acid (0.01 mol, 0.9449 g) in 25 mL of THF (Scheme 1) (Al-Heety & Al-Nasseri 2024; Benakli, Zha & Kerns 2001). A few drops of triethylamine were added as a catalyst, and the reaction mixture was refluxed with continuous stirring in a water bath at 70 °C for 1-15 h, depending on the nature of the imine substituent. The variation in reaction time was attributed to differences in the reactivity of the imine substrates under the applied reaction conditions. Therefore, the reaction time was adjusted for each substrate, and the reaction progress was monitored by thin-layer chromatography (TLC) using ethanol:ethyl acetate (7:3) until completion. Upon completion, the reaction mixture was cooled in an ice bath, and the resulting precipitate was collected by filtration. The products were obtained as black solids for **F1**, **F3**, and **F4** and as a brown solid for **F2**. The precipitates were washed with chloroform, recrystallized from absolute ethanol, and dried. The oxazolidinone derivatives were synthesized as illustrated in Scheme 1.

PROPERTIES AND CHARACTERIZATION OF SYNTHESIZED COMPOUNDS **(F1-F4)**

*Sodium 3-(3,4-dihydroxyphenyl)-2-(2-(4-hydroxy-3-methoxyphenyl)-5-oxooxazolidin-3-yl)-2-methylpropanoate (**F1**):*

Black solid; yield: 60%; M.wt.: 425.37 g/mol; mp: 195° C; Rf: 0.89; reaction time: 15 h; $C_{20}H_{20}NNaO_8$. FT-IR (ATR) (ν, cm^{-1}): 3506 (O-H); 3036 (C-H_{Ar}); 2924 (C-H_{alph}); 1581 (C=C_{Ar}); 1601 (COO_{asym}); 1313 (COO_{sym}); 1713 (C=$O_{lactone}$); 1381 ($CH_{2\ Sci}$); 1246 (C-O_{ph}); 1075 (C-N); 699 (C-H_{oop}); 1357 (C-O). ^{1}H-NMR (DMSO-d_6 400 MHz), δ, ppm: 1.19 (s, 3H, 2'-CH_3), 2.69-2.86 (dd, 2H, H-3'), 3.07-3.22 (dd, 2H, H-4), 3.88 (s, 3H, -OCH_3), 6.01 (s, 1H, H-2,



SCHEME 1. The general reaction of the oxazolidinone derivatives **F1-F4**

N-CH-O), 6.52-7.17 (m, d, 6H, Ar-H), 8.77 (s, 3H, Ar-OH). ^{13}C-NMR (DMSO-d_6 100 MHz), δ (ppm): 20.41 (4'-CH_3); 41.20 (C-3'); 51.64 (C-3); 57.17 (Ar-OCH_3); 67.95 (C-2', Me-C-N); 88.65 (C-2, N-C-O); 112.32, 115.50, 121.60, 129.76, 115.59, 116.60, 122.37, 129.07 (Ar-C); 144.38, 145.23, 149.00 (C-Ar); 147.47 (=C-OMe); 170.39 (C-1, O-CO lactone); 181.54 (C-1', -COO).

*Sodium 3-(3,4-dihydroxyphenyl)-2-(2-(4-hydroxyphenyl)-5-oxooxazolidin-3-yl)-2-methylpropanoate (**F2**):*

Brown solid; yield: 78%; M.wt.: 395.34 g/mol; mp: 106° C; Rf: 0.82; reaction time: 14 h; $C_{19}H_{18}NNaO_7$. FT-IR (ATR) (ν, cm^{-1}): 3400 (O-H); 3040 (C-H_{Ar}); 2983 (C-H_{alph}); 1579 (C=C_{Ar}); 1606 (COO_{asym}); 1211 (COO_{sym}); 1722 (C=$O_{lactone}$); 1387 (CH_{2Sci}); 1242 (C-O_{ph}); 1099 (C-N); 721 (C-H_{oop}); 1355 (C-O). ^{1}H-NMR (DMSO-d_6 400 MHz), δ, ppm: 1.08 (s, 3H, 2'-CH_3), 3.08-3.20 (dd, 2H, H-3'), 3.41-3.49 (dd, 2H, H-4), 5.94-6.03 (t, 3H, Ar-H), 6.15 (s, 1H, H-2, N-CH-O), 6.75-6.89 (m, 4H, Ar-H), 8.34 (s, 2H, Ar-OH), 8.67 (s, 1H, Ar-OH). ^{13}C-NMR (DMSO-d_6 100 MHz), δ (ppm): 21.15 (2'-CH_3); 41.62 (C-3'); 50.71 (C-5); 65.80 (C-4', Me-C-N); 92.20 (C-2, N-C-O); 116.16, 116.76, 121.03, 128.07, 115.49, 128.68, 130.16 (Ar-C); 144.59, 145.45, 157.76 (=C-OH); 171.69 (C-4, O-CO lactone); 183.60 (C-1', -COO).

*Sodium 2-(2-(4-bromophenyl)-2-methyl-5-oxooxazolidin-3-yl)-3-(3,4-dihydroxyphenyl)-2-methylpropanoate (**F3**):*

Black solid; yield: 67%; M.wt: 472.27 g/mol; mp: 150° C; Rf: 0.69; reaction time: 1 h; $C_{20}H_{19}BrNNaO_6$. FT-IR (ATR) (ν, cm^{-1}): 3477 (O-H); 3032 (C-H_{Ar}); 2949 (C-H_{alph}); 1532 (C=C_{Ar}); 1615 (COO_{asym}); 1330 (COO_{sym}); 1732 (C=$O_{lactone}$); 1394 ($CH_{2\ Sci}$); 1257 (C-O_{ph}); 1062 (C-N); 702 (C-H_{oop}); 1377 (C-O); 1050 (C-Br). ^{1}H-NMR (DMSO-d_6 400 MHz), δ, ppm: 1.15 (s, 3H, 2'-CH_3), 1.47 (s, 3H, 2-CH_3), 2.90-2.95 (dd, 2H, H-3'), 3.99-4.11 (dd, 2H, H-4), 6.58-6.66 (m, 3H, Ar-H), 7.74-7.91 (dd, 4H, Ar-H), 8.75 (s, 2H, Ar-OH). ^{13}C-NMR (DMSO-d_6 100 MHz), δ (ppm): 22.98 (2'-CH_3); 27.41 (1-CH_3); 43.20 (C-3'); 49.02 (C-4); 65.29 (C-4', Me-C-N); 101.61 (C-2, N-C-O); 116.11, 117.35, 120.74, 129.25, 126.59, 131.98, 140.47 (Ar-C); 123.47 (=C-Br); 144.51, 145.76 (=C-OH); 170.09 (C-5, O-CO lactone); 181.46 (C-1', -COO).

*Sodium 3-(3,4-dihydroxyphenyl)-2-methyl-2-(2-methyl-5-oxo-2-phenyloxazolidin-3-yl) propanoate (**F4**):*

Black solid; yield: 65%; M.wt: 393.37 g/mol; mp: 280° C; Rf: 0.73; reaction time: 1 h; $C_{20}H_{20}NNaO_6$. FT-IR (ATR) (ν, cm^{-1}): 3547 (O-H); 3035 (C-H_{Ar}); 2989 (C-H_{alph}); 1595 (C=C_{Ar}); 1610 (COO_{asym}); 1313 (COO_{sym}); 1719 (C=$O_{lactone}$); 1393 ($CH_{2\ Sci}$); 1281 (C-O_{ph}); 1090 (C-N); 761 (C-H_{oop}); 1360 (C-O). ^{1}H-NMR (400 MHz, DMSO-d_6), δ, ppm: 1.25 (s, 3H, 2'-CH_3), 1.52 (s, 3H, 2-CH_3), 2.67-2.73 (dd, 2H, H-3'), 3.05-3.11 (dd, 2H, H-4), 6.46-6.67 (d, s, 3H, Ar-H), 7.27-7.40 (dd, 5H, Ar-H), 8.71 (s, 2H, Ar-OH). ^{13}C-NMR (DMSO-d_6 100 MHz), δ (ppm): 21.23 (2'-CH_3); 25.30 (2-CH_3); 42.15 (C-3'); 48.09 (C-4); 61.36 (C-3, Me-C-N); 100.30 (C-2, N-C-O); 115.40, 121.64, 128.79, 117.35, 127.28, 129.49, 125.73, 140.02 (Ar-C); 144.51, 145.24 (=C-OH); 173.45 (C-5, O-CO lactone); 181.26 (C-1', -COO).

DETAILS OF THE COMPUTATION AND METHODOLOGY

Theoretical calculations are employed to assess the chemical characteristics of molecules by quantifying several chemical parameters. Every determined parameter offers details on several molecular features. To compute these parameters, Gaussian09 RevD.01 and GaussView 6.0 (Becke 1992; Dennington, Keith & Millam 2016; Frisch 2009) were utilized. The B3LYP/6-311G basis set was used for DFT computations (Günsel et al. 2019a; Vautherin & Brink 1972). Optimized structure, HOMO, LUMO, ΔE (HOMO-LUMO energy gap), dipole moment (D), softness (S), hardness (η) and electronegativity (χ) were among the characteristics that were computed by the formulas cited in the literature (Güzel et al. 2019; Tüzün 2018).

MOLECULAR DOCKING

Docking simulations were conducted using Chimera and AutoDock Vina, and the resulting interactions were visualized with Discovery Studio software. The docking studies focused on the complexes formed between the synthesized ligands and the bacterial DNA gyrase protein. The crystal structure of the target protein (PDB: 6f86) was obtained from the Protein Data Bank. Before the docking, all ligand and solvent molecules were removed from the original protein structure. Gasteiger charges and energy minimization were performed as part of the preparation protocol. All other parameters were kept at their default values. To ensure the reliability of the result, a minimum of five independent docking runs were conducted for each compound.

IN VITRO ANTIBACTERIAL ASSAY

The medium was prepared using Mueller-Hinton agar. The stock solutions were made by dissolving the synthesized compounds in DMSO along with the standards. *Cefotaxime sodium* was used as the reference standard. For twenty-four hours, the Petri dishes were incubated at 37 °C in an air environment. The diameter of the inhibition zone was measured and compared with the zones generated by the reference standard (Ragi et al. 2021).

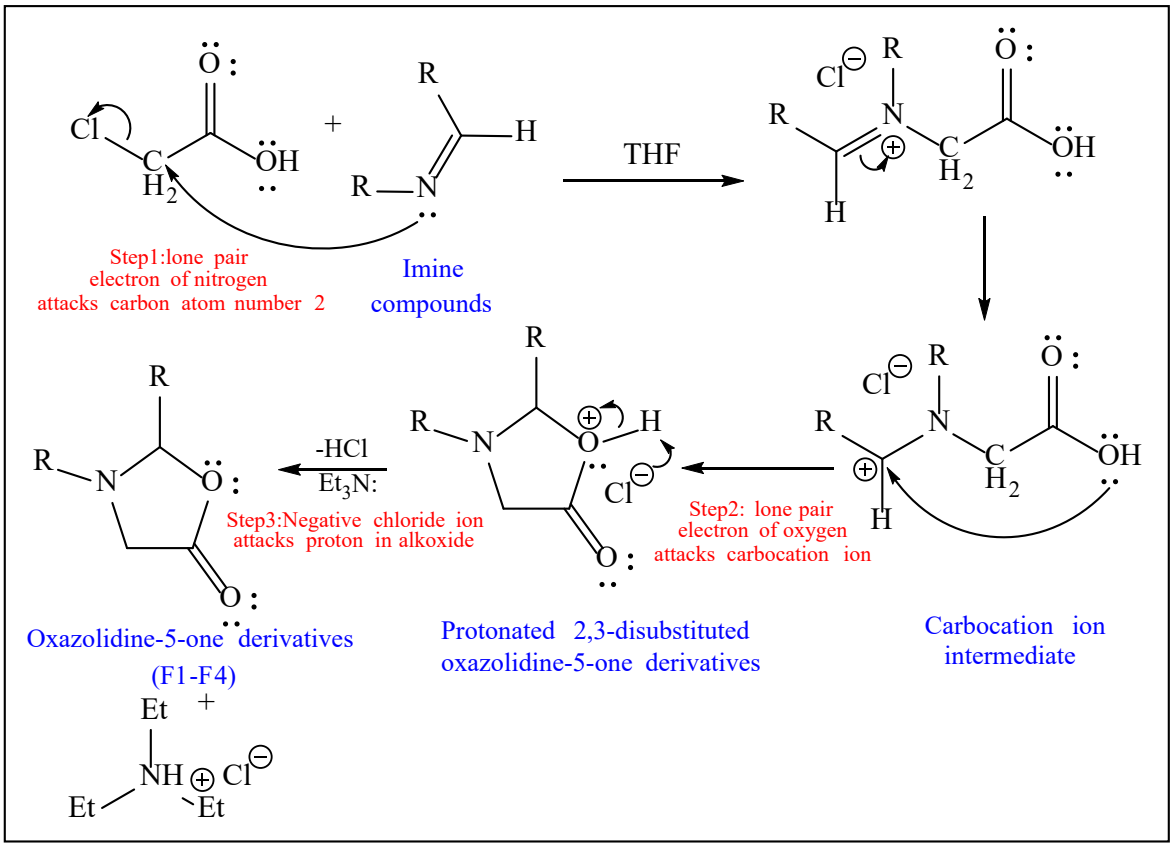
RESULTS AND DISCUSSION

THE PROPOSED MECHANISM OF THE SYNTHESIS OF OXAZOLIDINONE DERIVATIVES **F1-F4**

The proposed reaction mechanism of the oxazolidin-3-yl derivatives follows through multiple steps that involve imine intermediates and electrophilic activation. As illustrated in Scheme 2, the initial step involves a nucleophilic attack of the nitrogen electron pair of the imine compound on the electrophilic carbon atom, leading to the formation of C-N. During this step, the chloride ion departs as a leaving group. After that, a carbocation intermediate is formed, which allows nucleophilic attack via oxygen lone pair on the carbocation. This attack leads to the formation of the oxazolidine ring. Furthermore, the role of triethylamine as a base is to liberate chloride ion and capture it as triethylammonium chloride (Harwood & Pyriadi 1971) and then lead to the formation of the final product.

FOURIER-TRANSFORM INFRARED SPECTROSCOPY (FT-IR)

The FT-IR spectra of the synthesized compounds **F1-F4** exhibited characteristic absorption bands at 1713 cm^{-1}, 1722 cm^{-1}, 1719 cm^{-1}, and 1728 cm^{-1}, respectively, corresponding to the lactone carbonyl



SCHEME 2. General mechanism of synthesized compounds **F1-F4**

(C=O) stretching vibration of the oxazolidinone ring. Additionally, the presence of the carboxylate group (COO^-) was confirmed by asymmetric stretching bands observed at 1601 cm^{-1}, 1607 cm^{-1}, 1610 cm^{-1}, and 1610 cm^{-1}, and symmetric stretching bands observed at 1313 cm^{-1}, 1211 cm^{-1}, 1330 cm^{-1}, and 1313 cm^{-1}, respectively. The bands observed at 3547-3400 cm^{-1} region indicated the presence of (O-H) stretching vibrations of the phenolic groups. The successful formation of the oxazolidinone derivatives was confirmed by disappearance of the imine (C=N) stretching, which appears in the region of 1690-1640 cm^{-1} in the precursor compounds. Another interesting peak that confirms the formation of the oxazolidinone ring is the C-N stretching, which exhibits sharp and shoulder peaks at 1060 and 1099 cm^{-1} (Demir et al. 2020), as shown in Figure 1. Additionally, the **F3** compound showed a band at 1050 cm^{-1}, which confirmed the presence of C-Br bond.

PROTON NUCLEAR MAGNETIC RESONANCE SPECTROSCOPY (^{1}H-NMR)

The ^{1}H-NMR spectra (Figure 2) of the compounds **F1-F4** showed singlet peaks between 1.08-1.25 ppm, which indicates the presence of a tertiary methyl group (CH_3) attached to a quaternary carbon next to the carboxyl group. Two singlet peaks in the **F3** and **F4** spectra at 1.47 and 1.52 ppm also showed that the methyl group (CH_3) was attached to the oxazolidinone ring, confirming alkyl substitution on the heterocyclic ring. Also, methylene protons (CH_2) located adjacent to nitrogen and carbonyl in the oxazolidinone ring were found between 2.67 and 3.22 ppm of all compounds. The N-CH-O protons in the **F1** and **F2** compounds showed at 6.01-6.15 ppm, providing additional evidence for the formation of the oxazolidinone ring. Additionally, phenolic OH protons appear between the 8.67-8.77 ppm range, confirming the presence of a hydroxyl group.

CARBON NUCLEAR MAGNETIC RESONANCE SPECTROSCOPY (^{13}C-NMR)

The ^{13}C-NMR spectra (Figure 3) of **F1-F4** confirmed the structures of the synthesized compounds through the exhibition of distinctive carbon peaks. **F1-F4** compounds exhibited signals in the range of 20.4-22.9 ppm, attributed to a methyl group (CH_3) bound to a quaternary carbon adjacent to the carboxyl group. On the other hand, the secondary methyl carbon signals on the oxazolidinone ring of **F3** and **F4** appear at 25.3 and 27.4 ppm, respectively. Additionally, the methylene carbon (CH_2) adjacent to nitrogen and carbonyl groups within the oxazolidinone ring was observed between 48.0 and 51.6 ppm of all compounds, while the quaternary carbon bonded to nitrogen and methyl groups (CH_3-C-N) appeared at 67.9, 65.8, 65.2, and 61.3 ppm, respectively. The carbon of N-C-O within the oxazolidinone ring showed a range of 88.6-101.6 ppm for all the

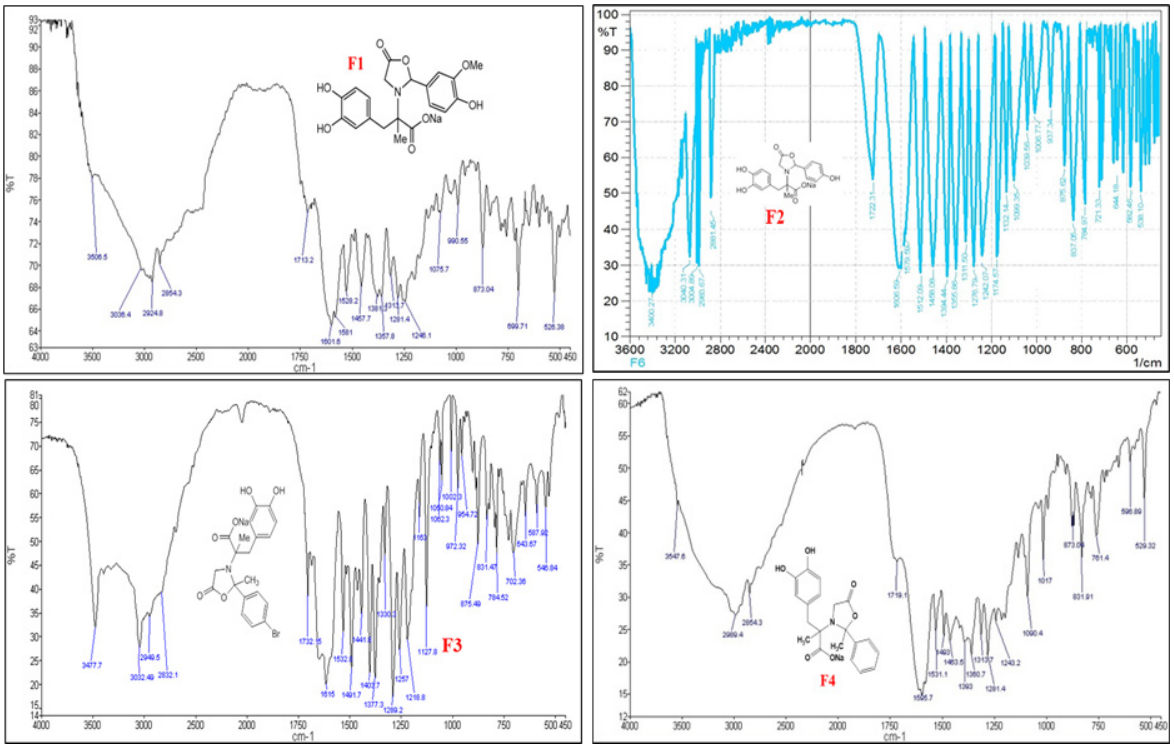


FIGURE 1. FT-IR spectra of **F1-F4** compounds

synthesized compounds. The methoxy-substituted derivative **F1** exhibited a signal at 57.1 ppm, attributed to the aromatic methoxy group (O-CH_3). Moreover, a significant observation is the appearance of distinctive carbonyl signals of the lactone group (C=O) within the oxazolidinone ring at 170.3, 171.6, 170.0, and 173.4 ppm, respectively, which provides an essential indicator for the successful synthesis of the heterocyclic lactone ring. This is supported by the disappearance of the imine (C=N) carbon signal, which typically appears in the region of 164-169 ppm in the precursor compounds (Jin et al. 2022), thus, highlighting the complete transformation of the starting materials into the oxazolidinone derivatives.

THEORETICAL CALCULATIONS

Those quantum parameters, which have gained increased significance and were calculated in Gaussian calculations, are HOMO (highest occupied molecular orbital) and it shows that the molecule has a tendency to donate electrons (Ojha, Tüzün & Bhawsar 2020), while LUMO (lowest unoccupied molecular orbital) shows that the molecule has a tendency to accept electrons (Günsel et al. 2019a). Table 1 represents HOMO, LUMO, and the optimized shapes of oxazolidinone derivatives (**F1**–**F4**). Table 2 presents the quantum chemical parameters calculated from DFT computations for oxazolidinone derivatives (**F1**–**F4**). Since each calculated parameter explains a different feature, each has a different importance, where the ΔE energy gap value is a parameter that indicates the activity of the molecule. The lower the ΔE energy gap value of a molecule, the more active it is. Another important parameter calculated is electronegativity. It describes the ability of an atom in a molecule to attract bonding electrons (Khalilov et al. 2021; Ojha, Tüzün & Bhawsar 2020). A greater numerical value for this parameter indicates that the atoms in the molecule will attract more bond electrons, lowering the molecule's activity (Günsel et al. 2019b). The hardness and softness characteristics of molecules are two additional crucial factors. Because hard molecules find it difficult to transfer electrons to an acceptor, they are less reactive than soft molecules (Khalilov et al. 2021). According to Gaussian calculations, compound **F4** is the most reactive, while compound **F3** is the most stable.

The HOMO and LUMO distributions provide additional insight into the electronic characteristics of the synthesized oxazolidinone derivatives (Table 1). Frontier molecular orbital analysis is useful for describing the spatial distribution of electron density and the electronic effects associated with structural modifications

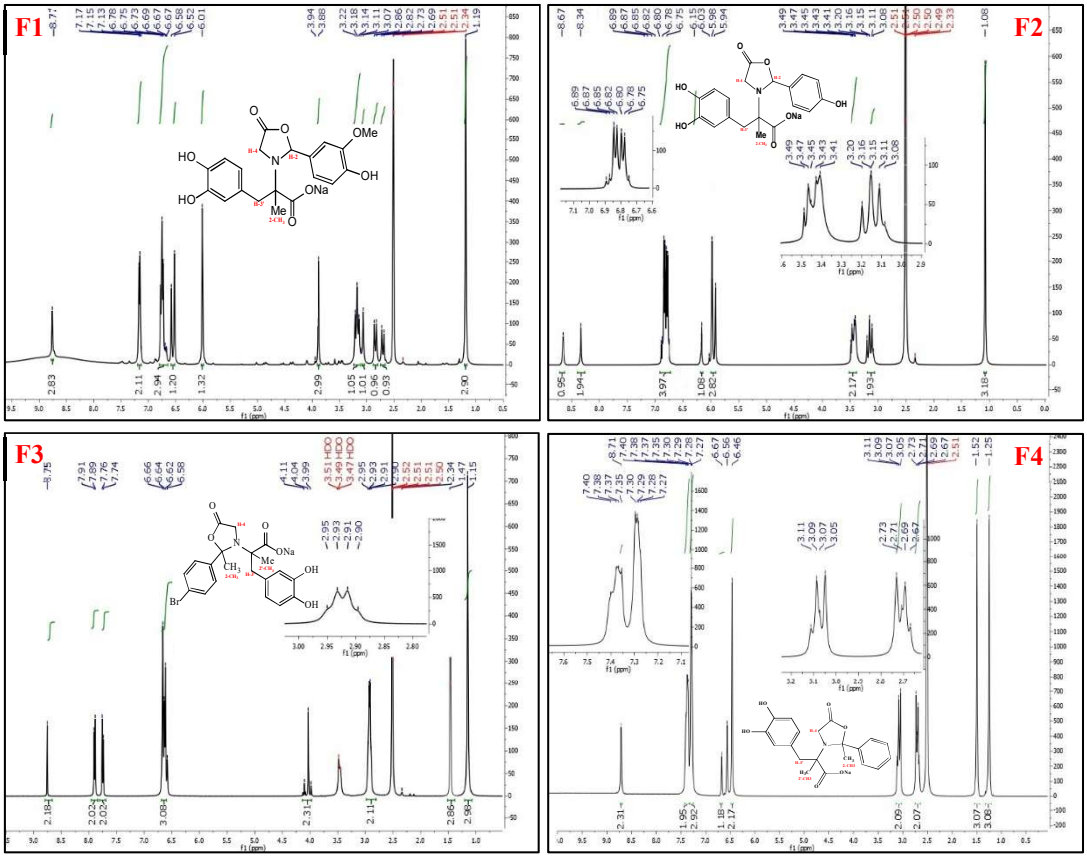


FIGURE 2. ^{1}H-NMR spectra of **F1**–**F4** compounds in DMSO-d_6

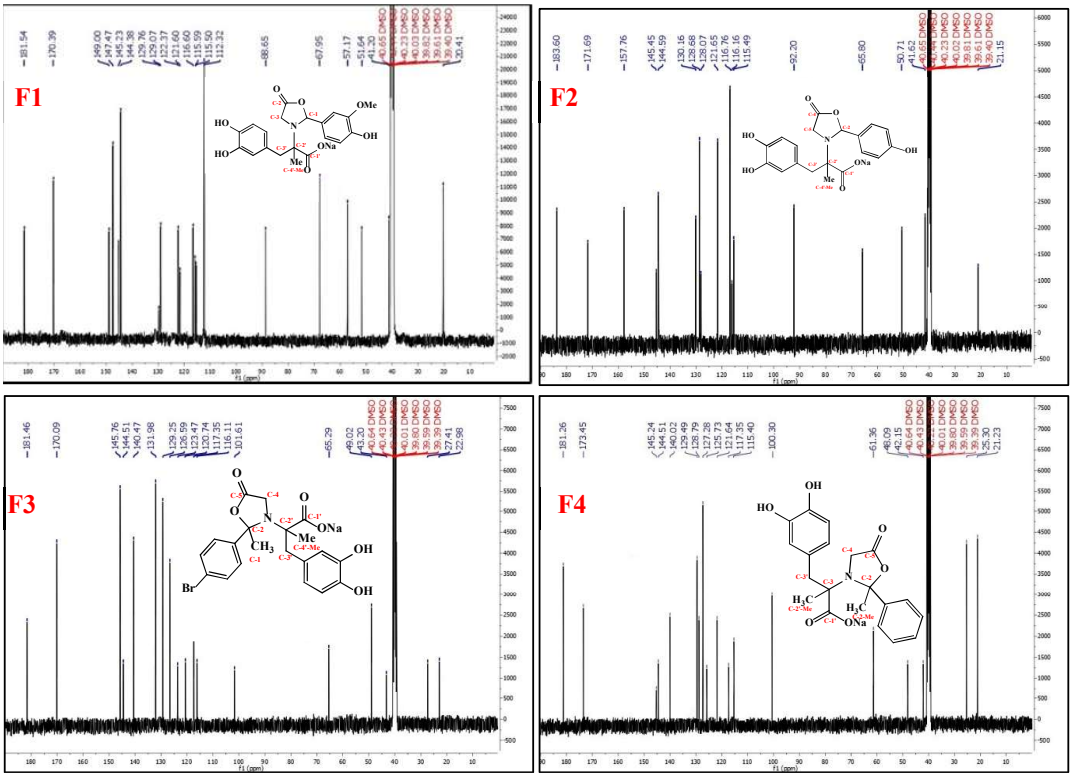


FIGURE 3. ^{13}C-NMR spectra of **F1**–**F4** compounds in DMSO-d_6

and substituents. For **F1** and **F2**, the HOMO density is mainly localized over the aromatic and central portions of the molecules, whereas the LUMO exhibits a more diffuse distribution extending toward other regions of the molecular framework. A similar spatial redistribution is observed for **F3**, where the HOMO is predominantly distributed over the aromatic and central portions, while the LUMO is more localized toward the opposite side of the molecule, particularly near the bromophenyl-substituted region. In **F4**, the HOMO is distributed over several portions of the molecular framework, whereas the LUMO shows a more distinct localization in a region different from that predominantly occupied by the HOMO. These differences indicate that the HOMO-to-LUMO transition is associated with a redistribution in the spatial localization of electron density within the molecular framework, and that the nature of the substituents influences the distribution of the frontier molecular orbitals. Similar substituent-dependent changes in HOMO and LUMO localization have been reported for oxazolidinone derivatives, supporting the relevance of frontier-orbital analysis for interpreting the electronic effects of structural modification (Soni et al. 2025).

The calculated HOMO–LUMO energy gaps further support the differences in the electronic properties of the compounds. **F4** exhibited the smallest energy gap (3.478 eV), indicating a relatively smaller energetic separation between the frontier orbitals and a comparatively greater ease of electronic excitation than **F1** (4.737 eV), **F2** (4.728 eV), and **F3** (7.768 eV). In contrast, **F3** showed the largest energy gap, indicating comparatively greater electronic stability among the investigated derivatives. The relationship between the HOMO–LUMO gap and molecular electronic properties has been widely used in DFT-based molecular analysis, with smaller gaps generally associated with greater softness and chemical reactivity, whereas larger gaps are associated with greater hardness and relative stability (Yoo et al. 2023). Overall, the combination of the frontier-orbital distributions and the calculated HOMO–LUMO gaps demonstrates that structural modification of the oxazolidinone scaffold influences the electronic properties and spatial distribution of the frontier molecular orbitals.

MOLECULAR DOCKING ANALYSIS

Bacterial DNA gyrase is a heterotetrameric enzyme composed of two GyrA and two GyrB subunits. Together, these subunits form three pairs of gates that sequentially open and close, enabling the passage of a DNA segment and the introduction of two negative supercoils (Gutierrez et al. 2024; Vanden Broeck et al. 2019). Among these, the most notable gate is the N-gate of GyrB subunits, which contains an ATPase domain responsible for binding and hydrolysis of ATP to drive the supercoiling process. This domain is lined within residues Lys-103 and Lys-110; furthermore, certain

TABLE 1. HOMO and LUMO frontier molecular orbital distributions and optimized molecular structures of the synthesized oxazolidinone derivatives (**F1-F4**)

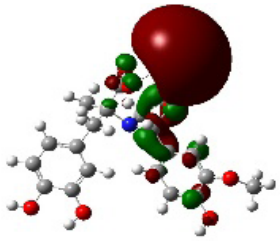
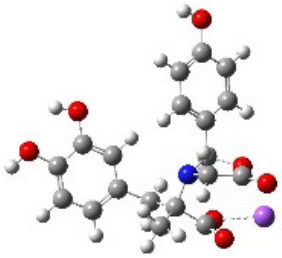
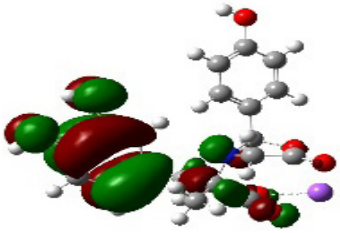
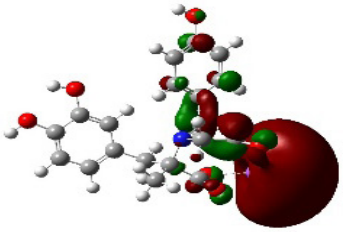
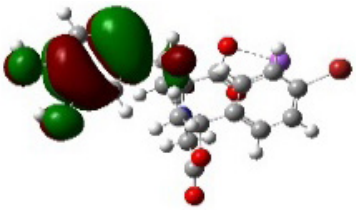
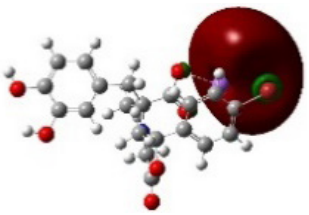
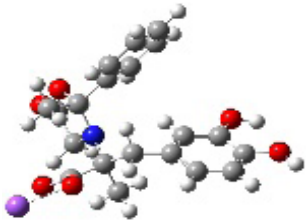
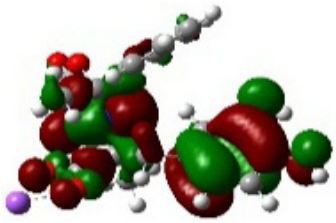
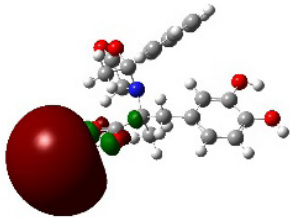
 **F1**	 HOMO	 LUMO
 **F2**	 HOMO	 LUMO
 **F3**	 HOMO	 LUMO
 **F4**	 HOMO	 LUMO

TABLE 2. The quantum chemical parameters calculated from DFT computations for (**F1-F4**) compounds

No.	HOMO eV	LUMO eV	ΔE eV	D Deby	S eV^{-1}	h eV	c eV
F1	-5.671	-0.934	4.737	2.82	0.422	2.3685	3.3025
F2	-5.692	-0.964	4.728	2.32	0.423	2.364	3.328
F3	-8.332	-0.564	7.768	8.28	0.258	3.884	4.448
F4	-5.342	-1.864	3.478	11.02	0.575	1.739	3.603

amino acid residues such as GyrB P79, K103, E42, N46, and E50 are involved in coupling ATP hydrolysis to DNA supercoiling (Gross et al. 2003; Tamura & Gellert 1990). The GyrB subunit is a major focus as a drug target not only due to its role in the bacterial DNA replication cycle, but also due to its absence in mammalian organisms, making it a promising and selective target for antibacterial therapies (Collin, Karkare & Maxwell 2011; Gutierrez et al. 2024; Maxwell 1997).

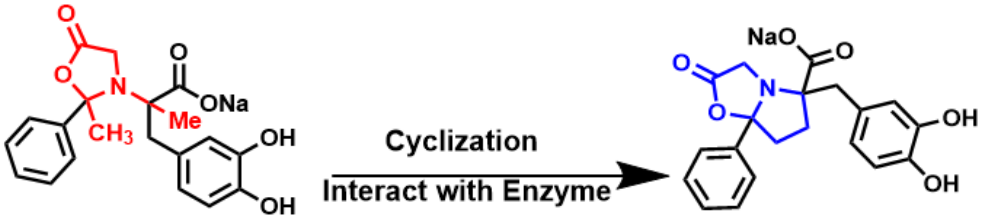
The docking analysis of compound **F1** shows seven non-bonding interactions with various amino acids. A careful inspection of the binding pocket indicated that **F1** adopted a position in free space directed toward the hydrophobic (C-terminal) region and enclosed by the ATPase domain (Figure 4(a)). The binding includes hydrogen bonds with residues Arg76, ASN46, and Gly77, with interaction distances ranging from 1.9Å to 3.5Å. Additionally, hydrophobic interactions are observed with Ile78 and Pro79. A salt-bridge electrostatic interaction occurs between the planar aromatic ring of **F1** and residues Glu50 and Arg76, which contribute to stabilizing the ligands at the binding site (Lamut et al. 2020; Tomašič et al. 2015), as shown in Figure 4(b). The docking score of the interaction was -7.1 kcal/mol. The binding pocket volume radius was 9.8 Å. Compound **F2** shows the main interaction, via a hydrogen bond between Gly77 and the hydroxyl group substituted on the benzyl ring, with a distance of 2.5Å. Other interactions were one electrostatic and two hydrophobic with Glu50, Ile78, and Pro79 (Figure 4(C)), respectively. The position of the binding pocket was similar to compound **F1** (Figure 4(D)), with a volume radius of 8.8Å, and binding energy -7.1 kcal/mol. An interesting observation was made for compounds **F3** and **F4**, which underwent cyclization between the methyl oxazolidine ring and 2-methylpropanoate during interaction with the enzyme to form a new fused heterocyclic structure oxohexahydropyrrolo[2,1-b]oxazole (Scheme 3). Although this intramolecular cyclization did not significantly alter the overall interaction pattern with the enzyme, the binding behavior remained comparable to that of compound **F1** (Figure 4(E) & 4(F)). A slight reduction in the binding pocket volume was noted, measuring approximately 7.8Å. Both compounds **F3** and **F4** formed hydrogen bonds with residue Asp73, Arg76, and Gly77, with an average bond length of 2.5Å. additionally, electrostatic and hydrophobic interaction were observed with Glu50, Ile78, and Pro79 (Figure 4(G)), respectively.

ANTIBACTERIAL ACTIVITIES

Derivatives of oxazolidinone (**F1**–**F4**) were evaluated against *Streptococcus* spp., *Pseudomonas aeruginosa*, *Staphylococcus aureus*, and *Escherichia coli*. The oxazolidinone derivatives were incubated for 24 h at 37 °C at concentrations of 1.25 and 2.5 mg/mL in dimethyl sulfoxide (DMSO). Cefotaxime sodium was employed as the standard reference. The results showed a range of antibacterial activity among the oxazolidinone derivatives. Compound **F3** showed the highest activity among the synthesized derivatives against *Escherichia coli* at both concentrations, with inhibition zones close to those of the reference standard. Compound **F2** also showed strong antibacterial activity against *Escherichia coli* at both concentrations, although its inhibition zones were lower than those of cefotaxime sodium. The inhibition zones observed for all tested compounds and bacterial strains are presented in Table 3.

The antibacterial activity of compounds **F1**–**F4** showed clear differences depending on both the structural features of the derivatives and the bacterial strain. Among the tested compounds, **F3** exhibited the highest activity against the Gram-negative bacteria, particularly *Escherichia coli*, producing inhibition zones of 31 and 35 mm at 1.25 and 2.5 mg/mL, respectively, which were close to those produced by cefotaxime sodium (32 and 36 mm). **F4** also showed strong activity against *E. coli* (29 and 30 mm), followed by **F2** (27 and 29 mm), whereas **F1** exhibited the lowest activity (19 and 21 mm). A similar trend was observed against *Pseudomonas aeruginosa*, where **F3** and **F4** showed higher activity than **F2**, while **F1** displayed no detectable activity at 1.25 mg/mL and only limited activity at 2.5 mg/mL. These results suggest that the structural modifications introduced into the oxazolidinone scaffold influence the antibacterial response, particularly against Gram-negative bacteria.

The structural differences among **F1**–**F4** may contribute to the observed variation in activity. **F1** contains a 4-hydroxy-3-methoxyphenyl substituent, whereas **F2** contains a 4-hydroxyphenyl group without the methoxy



SCHEME 3. Intramolecular cyclization of compounds **F3** & **F4** during the interaction with the enzyme

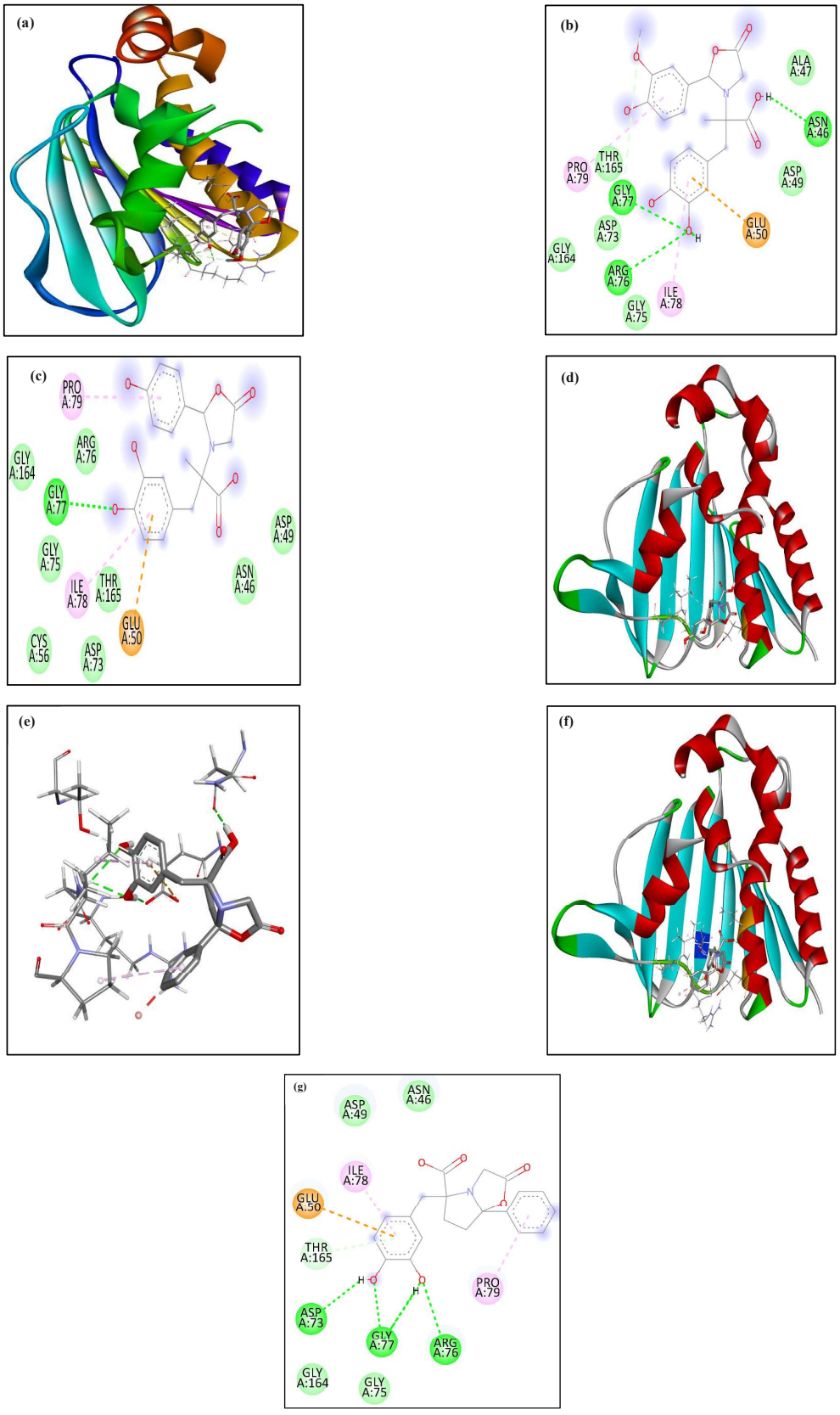


FIGURE 4. (a): Ccavities are occupied by the ligand **F1** in free space directed toward the hydrophobic (C-terminal) region and enclosed by the ATPase domain, (b & c): 2D diagram interaction of bacterial DNA gyrase with ligand **F1** and **F2**, respectively, (d): docking of ligand **F2** on the enzyme surface, (e): docking results of **F3** with the active site of the enzyme, (f): interaction of **F3** in the active site on the enzyme surface, and (g): 2D diagram interaction of bacterial DNA gyrase with ligand **F3**

TABLE 3. Antibacterial activity of oxazolidinone derivatives (**F1**–**F4**) against selected Gram-positive and Gram-negative bacteria, expressed as inhibition zones (mm) at 1.25 and 2.5 mg/mL

Bacterial strain	Compound	Inhibition zone (mm) at 1.25 mg/mL	Inhibition zone (mm) at 2.5 mg/mL
Escherichia coli	**F1**	19	21
	F2	27	29
	F3	31	35
	F4	29	30
	Standard**	32	36
Pseudomonas aeruginosa	**F1**	*	11
	F2	15	21
	F3	19	25
	F4	20	22
	Standard**	29	34
Staphylococcus aureus	**F1**	8	10
	F2	18	21
	F3	14	16
	F4	10	14
	Standard**	18	23
Streptococcus spp.	**F1**	*	*
	F2	15	20
	F3	18	21
	F4	12	16
	Standard**	20	25

*No bacterial growth was observed. **Cefotaxime sodium was used as standard

substituent. Despite this difference, **F2** showed higher activity than **F1** against all tested bacterial strains for which inhibition was observed, suggesting that removal of the methoxy group may favor the antibacterial activity of this series. **F3** and **F4** contain an additional methyl group associated with the oxazolidinone framework, while **F3** additionally possesses a 4-bromophenyl substituent. The presence of the bromine-containing aromatic substituent in **F3** was associated with particularly strong activity against *E. coli* and *P. aeruginosa*. However, the activity pattern was strain-dependent, since **F2** showed the highest activity against the Gram-positive *Staphylococcus aureus*, with inhibition zones of 18 and 21 mm, while **F3** showed moderate activity (14 and 16 mm). Against *Streptococcus* spp., **F3** showed the highest activity among the synthesized derivatives (18 and 21 mm), followed by **F2** and **F4**, whereas **F1** showed no detectable activity. These findings indicate that the effect of structural modification is dependent not only on the substituent pattern but also on the bacterial strain.

The antibacterial results can be further considered in relation to the molecular docking analysis against bacterial DNA gyrase. Compounds **F3** and **F4** exhibited interactions with the ATPase binding region involving hydrogen bonds with Asp73, Arg76, and Gly77, together with electrostatic and hydrophobic interactions involving Glu50, Ile78, and Pro79. The presence of these multiple non-covalent interactions may contribute to the favorable binding of these derivatives within the enzyme binding pocket. Notably, **F3**, which exhibited the highest antibacterial activity against *E. coli*, showed this extensive interaction pattern, providing a possible molecular explanation for its strong activity against this strain. **F2** also showed a favorable docking score of −7.1 kcal/mol and formed a hydrogen bond with Gly77 through its hydroxyl group, in addition to electrostatic and hydrophobic interactions with Glu50, Ile78, and Pro79. This is consistent with its relatively strong antibacterial activity, particularly against *S. aureus*. Nevertheless, the antibacterial results do not follow the docking results in a strictly quantitative manner, indicating that factors other than binding affinity, including substituent-dependent molecular properties and bacterial strain characteristics, may also influence the observed activity. Overall, the antibacterial and docking results together suggest that structural modification of the oxazolidinone scaffold can affect both the biological response of the compounds and their interactions with the bacterial DNA gyrase binding site.

CONCLUSION

In this study, new oxazolidinone derivatives (**F1**–**F4**) were successfully synthesized. The structures of the (**F1**-**F4**) compounds were confirmed using FT-IR, ^{1}H-NMR, and ^{13}C-NMR spectroscopy. DFT (B3LYP/6-311G) showed the electronic properties of the compounds. The results showed that compound **F4** had the smallest HOMO-LUMO energy gap, which means it was more reactive, while **F3** was more stable. Molecular docking studies against bacterial DNA gyrase (PDB ID: 6f86) showed that **F3** and **F4** had high binding affinities, due to multiple hydrogen bonding and hydrophobic interactions. The *in vitro* antibacterial evaluation also showed that these compounds have promising activity. These results suggest that the oxazolidinone derivatives that were synthesized could be candidates for the further development of antibacterial agents that target DNA gyrase.

ACKNOWLEDGEMENTS

We gratefully acknowledge support received from the Department of Chemistry at the University of Anbar College of Science and the Universiti Kebangsaan Malaysia under Geran Universiti Penyelidikan (GUP-2025-040).

REFERENCES

Al-Heety, Z.A. & Al-Nasseri, A.K. 2024. Synthesis and characterization of new spiroheterocyclic from isatin and evaluation of its antifungal and antibacterial activity. *Synthesis* 18(02): 88-95.

Becke, A.D. 1992. Density-functional thermochemistry. I. The effect of the exchange-only gradient correction. *The Journal of Chemical Physics* 96(3): 2155-2160.

Benakli, K., Zha, C. & Kerns, R.J. 2001. Oxazolidinone protected 2-amino-2-deoxy-D-glucose derivatives as versatile intermediates in stereoselective oligosaccharide synthesis and the formation of α-linked glycosides. *Journal of the American Chemical Society* 123(38): 9461-9462.

Bouzina, A., Berredjem, M., Bouacida, S., Bachari, K., Marminon, C., Le Borgne, M., Bouaziz, Z. & Bouone, Y.O. 2022. Synthesis, *in silico* study (DFT, ADMET) and crystal structure of novel sulfamoyloxy-oxazolidinones: Interaction with SARS-CoV-2. *Journal of Molecular Structure* 1257: 132579.

Carena, A.A. & Stryjewski, M.E. 2020. Tedizolid (torezolid) for the treatment of complicated skin and skin structure infections. *Expert Review of Clinical Pharmacology* 13(6): 577-592.

Collin, F., Karkare, S. & Maxwell, A. 2011. Exploiting bacterial DNA gyrase as a drug target: Current state and perspectives. *Applied Microbiology and Biotechnology* 92(3): 479-497. doi:10.1007/s00253-011-3557-z

Demir, E., Sari, O., Çetinkaya, Y., Atmaca, U., Erdem, S.S. & Çelik, M. 2020. One-pot synthesis of oxazolidinones and five-membered cyclic carbonates from epoxides and chlorosulfonyl isocyanate: Theoretical evidence for an asynchronous concerted pathway. *Beilstein Journal of Organic Chemistry* 16(1): 1805-1819.

Dennington, R., Keith, T.A. & Millam, J.M. 2016. *GaussView 6.0. 16.* Semichem Inc.: Shawnee Mission, KS, USA. pp. 143-150.

Fernandes, G.F.S., Scarim, C.B., Kim, S-H., Wu, J. & Castagnolo, D. 2023. Oxazolidinones as versatile scaffolds in medicinal chemistry. *RSC Medicinal Chemistry* 14(5): 823-847.

Foti, C., Piperno, A., Scala, A. & Giuffrè, O. 2021. Oxazolidinone antibiotics: Chemical, biological and analytical aspects. *Molecules* 26(14): 4280.

Frisch, A. 2009. *gaussian 09W Reference*. Wallingford, USA. 25p 470.

Fujimoto, J., Okamoto, R., Noguchi, N., Hara, R., Masada, S., Kawamoto, T., Nagase, H., Tamura, Y.O., Imanishi, M., Takagahara, S., Kubo, K., Tohyama, K., Iida, K., Andou, T., Miyahisa, I., Matsui, J., Hayashi, R., Maekawa, T. & Matsunaga, N. 2017. Discovery of 3, 5-diphenyl-4-methyl-1, 3-oxazolidin-2-ones as novel, potent, and orally available Δ-5 desaturase (D5D) inhibitors. *Journal of Medicinal Chemistry* 60(21): 8963-8981.

Ganiu, M.O., Nepal, B., Van Houten, J.P. & Kartika, R. 2020. A decade review of triphosgene and its applications in organic reactions. *Tetrahedron* 76(47): 131553.

Ghosh, A.K., Williams, J.N., Ho, R.Y., Simpson, H.M., Hattori, S., Hayashi, H., Agniswamy, J., Wang, Y-F., Weber, I.T. & Mitsuya, H. 2018. Design and synthesis of potent HIV-1 protease inhibitors containing bicyclic oxazolidinone scaffold as the P2 ligands: Structure–activity studies and biological and X-ray structural studies. *Journal of Medicinal Chemistry* 61(21): 9722-9737.

Gross, C.H., Parsons, J.D., Grossman, T.H., Charifson, P.S., Bellon, S., Jernee, J., Dwyer, M., Chambers, S.P., Markland, W., Botfield, M. & Raybuck, S.A. 2003. Active-site residues of *Escherichia coli* DNA gyrase required in coupling ATP hydrolysis to DNA supercoiling and amino acid substitutions leading to novobiocin resistance. *Antimicrobial Agents and Chemotherapy* 47(3): 1037-1046. doi:10.1128/AAC.47.3.1037-1046.2003

Günsel, A., Bilgiçli, A.T., Pişkin, H., Tüzün, B., Yarasir, M.N. & Gündüz, B. 2019a. Synthesis of non-peripherally tetra-substituted copper (ii) phthalocyanines: Characterization, optical and surface properties, fabrication and photo-electrical properties of a photosensitive diode. *Dalton Transactions* 48(39): 14839-14852.

Günsel, A., Bilgicli, A.T., Tüzün, B., Pişkin, H., Atmaca, G.Y., Erdoğmuş, A. & Yarasir, M.N. 2019b. Synthesis of tetra-substituted phthalocyanines bearing 2-(ethyl (m-tolyl) amino) ethanol: Computational and photophysicochemical studies. *Journal of Photochemistry and Photobiology A: Chemistry* 373: 77-86.

Gutierrez, L., Peršolja, P., Tosso, R., Zidar, N., Kikelj, D. & Enriz, R.D. 2024. New ATP-competitive inhibitors of *E. coli* GyrB obtained from the mapping of the hydrophobic floor at the binding site: Synthesis and biological evaluation. *RSC Med. Chem.* 15(11): 3759-3777. doi:10.1039/D4MD00498A

Güzel, E., Günsel, A., Tüzün, B., Atmaca, G.Y., Bilgicli, A.T., Erdoğmuş, A. & Yarasir, M.N. 2019. Synthesis of tetra-substituted metallophthalocyanines: Spectral, structural, computational studies and investigation of their photophysical and photochemical properties. *Polyhedron* 158: 316-324.

Harwood, H.J. & Pyriadi, T.M. 1971. Use of acetyl chloride-triethylamine and acetic anhydride-triethylamine mixtures in the synthesis of isomaleimides from maleamic acids. *The Journal of Organic Chemistry* 36(6): 821-823.

Huang, H., Degnan, A.P., Balakrishnan, A., Easton, A., Gulianello, M., Huang, Y., Matchett, M., Mattson, G., Miller, R., Santone, K.S., Senapati, A., Shields, E.E., Sivarao, D.V., Snyder, L.B., Westphal, R., Whiterock, V.J., Yang, F., Bronson, J.J. & Macor, J.E. 2016. Oxazolidinone-based allosteric modulators of mGluR5: Defining molecular switches to create a pharmacological tool box. *Bioorganic & Medicinal Chemistry Letters* 26(17): 4165-4169.

Jin, B., Chen, J., Sheng, Z., Sun, M. & Yang, H. 2022. Synthesis, antibacterial and anthelmintic activity of novel 3-(3-pyridyl)-oxazolidinone-5-methyl ester derivatives. *Molecules* 27(3): 1103.

Khalilov, A.N., Tüzün, B., Taslimi, P., Tas, A., Tuncbilek, Z. & Cakmak, N.K. 2021. Cytotoxic effect, spectroscopy, DFT, enzyme inhibition, and moleculer docking studies of some novel mesitylaminopropanols: Antidiabetic and anticholinergics and anticancer potentials. *Journal of Molecular Liquids* 344: 117761.

Lamut, A., Skok, Ž., Barančoková, M., Gutierrez, L.J., Cruz, C.D., Tammela, P., Draskovits, G., Szili, P.E., Nyerges, Á., Pál, C., Molek, P., Bratkovič, T., Ilaš, J., Zidar, N., Zega, A., Enriz, R.D., Kikelj, D. & Tomašič, T. 2020. Second-generation 4,5,6,7-tetrahydrobenzo[*d*]thiazoles as novel DNA gyrase inhibitors. *Future Medicinal Chemistry* 12(4): 277-297. doi:10.4155/fmc-2019-0127

Leach, K.L., Brickner, S.J., Noe, M.C. & Miller, P.F. 2011. Linezolid, the first oxazolidinone antibacterial agent. *Annals of the New York Academy of Sciences* 1222(1): 49-54.

Malik, M.S., Faazil, S., Alsharif, M.A., Sajid Jamal, Q.M., Al-Fahemi, J.H., Banerjee, A., Chattopadhyay, A., Pal, S.K., Kamal, A. & Ahmed, S.A. 2023. Antibacterial properties and computational insights of potent novel linezolid-based oxazolidinones. *Pharmaceuticals* 16(4): 516.

Maxwell, A. 1997. DNA gyrase as a drug target. *Trends in Microbiology* 5(3): 102-109. doi:https://doi.org/10.1016/S0966-842X(96)10085-8

Ojha, L.K., Tüzün, B. & Bhawsar, J. 2020. Experimental and theoretical study of effect of *Allium sativum* extracts as corrosion inhibitor on mild steel in 1 M HCl medium. *Journal of bio-and tribo-corrosion* 6(2): 39.

Ragi, K., Kakkassery, J.T., Raphael, V.P., Johnson, R. & Thomas K., V. 2021. *In vitro* antibacterial and *in silico* docking studies of two Schiff bases on *Staphylococcus aureus* and its target proteins. *Future Journal of Pharmaceutical Sciences* 7(1): 78.

Rani, P., Das, R. & Nagaraja, C.M. 2025. A review on framework (MOF/COF/POP)-based materials for efficient conversion of CO_2 to bio-active oxazolidinones. *Inorganic Chemistry Frontiers* 12(2): 430-478.

Soni, S., Patil, K., Gavale, S., Pathan, S., Yadav, R., Murumkar, P.R. & Kadu, R. 2025. Exploring oxazolidinone scaffolds for future antibiotics: Synthesis and computational insights with DFT, docking, ADME and MD simulation. *Journal of Computer-Aided Molecular Design* 39(1): 58.

Tamura, J.K. & Gellert, M. 1990. Characterization of the ATP binding site on *Escherichia coli* DNA gyrase. Affinity labeling of Lys-103 and Lys-110 of the B subunit by pyridoxal 5'-diphospho-5'-adenosine. *The Journal of Biological Chemistry* 265(34): 21342-21349.

Tomašič, T., Katsamakas, S., Hodnik, Ž., Ilaš, J., Brvar, M., Solmajer, T., Montalvão, S., Tammela, P., Banjanac, M., Ergović, G., Anderluh, M., Mašič, L.P. & Kikelj, D. 2015. Discovery of 4,5,6,7-Tetrahydrobenzo[1,2-d]thiazoles as novel DNA gyrase inhibitors targeting the ATP-binding site. *Journal of Medicinal Chemistry* 58(14): 5501-5521. doi:10.1021/acs.jmedchem.5b00489

Tüzün, B. 2018. Theoretical evaluation of six indazole derivatives as corrosion inhibitors based on DFT. *Turkish Computational and Theoretical Chemistry* 2(1): 12-22.

Vanden Broeck, A., Lotz, C., Ortiz, J. & Lamour, V. 2019. Cryo-EM structure of the complete *E. coli* DNA gyrase nucleoprotein complex. *Nature Communications* 10(1): 4935. doi:10.1038/s41467-019-12914-y

Vautherin, D. & Brink, D.M. 1972. Hartree-Fock calculations with Skyrme's interaction. I. Spherical nuclei. *Physical Review C* 5(3): 626.

Yoo, P., Bhowmik, D., Mehta, K., Zhang, P., Liu, F., Lupo Pasini, M. & Irle, S. 2023. Deep learning workflow for the inverse design of molecules with specific optoelectronic properties. *Scientific Reports* 13(1): 20031.

Zhao, H., Wang, B., Fu, L., Li, G., Lu, H., Liu, Y., Sheng, L., Li, Y., Zhang, B., Lu, Y., Ma, C., Huang, H., Zhang, D. & Lu, Y. 2020. Discovery of a conformationally constrained oxazolidinone with improved safety and efficacy profiles for the treatment of multidrug-resistant tuberculosis. *Journal of Medicinal Chemistry* 63(17): 9316-9339.

Zhao, Q., Xin, L., Liu, Y., Liang, C., Li, J., Jian, Y., Li, H., Shi, Z., Liu, H. & Cao, W. 2021. Current landscape and future perspective of oxazolidinone scaffolds containing antibacterial drugs. *Journal of Medicinal Chemistry* 64(15): 10557-10580.